Molecular Crystals and Liquid Crystals Science and Technology. Section A. Molecular Crystals and Liquid Crystals

Publication details, including instructions for authors and subscription information:
http://www.tandfonline.com/loi/gmcl19

AFM in Organic Solid State Reactions

Gerd Kaupp [a], Jens Schmeyers [a], Michael Haak [a], Thorsten Marquardt [a] & Andreas Herrmann [a]

[a] University of Oldenburg, FB 9, - Organische Chemie I P.O. Box 2503, D-26111, Oldenburg, Germany

Version of record first published: 04 Oct 2006.

To cite this article: Gerd Kaupp , Jens Schmeyers , Michael Haak , Thorsten Marquardt & Andreas Herrmann (1996): AFM in Organic Solid State Reactions, Molecular Crystals and Liquid Crystals Science and Technology. Section A. Molecular Crystals and Liquid Crystals, 276:1-2, 315-337

To link to this article: http://dx.doi.org/10.1080/10587259608039392

Mol. Cryst. Liq. Cryst., 1996, Vol. 276, pp. 315–337
Reprints available directly from the publisher
Photocopying permitted by license only

AFM IN ORGANIC SOLID STATE REACTIONS

GERD KAUPP, JENS SCHMEYERS, MICHAEL HAAK, THORSTEN MARQUARDT, and ANDREAS HERRMANN
University of Oldenburg, FB 9, - Organische Chemie I - P.O. Box 2503, D-26111 Oldenburg, Germany

Abstract Organic solid-state reactions are probed with the atomic force microscope (AFM). In all cases phase rebuilding gives rise to characteristic submicroscopic features which change in shape due to phase transformation in later stages of the chemical reaction. Photo-(*E/Z*)-isomerization of olefin **1** occurs in the crystal, photodimerization of 9-chloroanthracene **3** is used as a probe for characterizing the luminosity distribution of SNOM-tips. Gas/solid imbibition in chiral host **5** proceeds enantiospecifically. Histidine crystals form the dihydrochloride with HCl, ammonia and methylamine react face-selectively with crystalline adipic acid **8**, furane-2-carboxylic acid **10** and 2-mercaptobenzothiazole **12**. Crystals of olefin **14** add chlorine. Solid-state diazotations and subsequent transformations of the solid diazonium nitrates into triazenes occur quantitatively. Solid/solid pinacol- and benzilic acid rearrangements are probed with the AFM. The features formed by long range molecular movements relate to the crystal packing and are thus different on different faces. Correlations with X-ray structural data are demonstrated. All reactions proceed to completion on a preparative scale and do not produce wastes as do their less selective counterparts if performed in solution.

Keywords: Organic solid-state reactions, AFM, SNOM-tip, imbibition, salt formations, chlorination, diazotations, triazene, gas/solid-reactions, solid/solid-reactions, crystal packing, waste-free reactions

INTRODUCTION

Atomic force microscopy (AFM) on organic solid state photolyses and gas/solid reactions revealed anisotropic long range molecular movements with formation of one out of 8

basic types of features.[1,2] Topochemistry[3] did not foresee such behavior, but it is now evident, that movements of molecules over tens and hundreds of nm are of major importance for the solid-state reactivity, and also the numerous exceptions to the topochemical postulate are well settled with the new principle of *phase rebuilding*,[1,2] which indicates the formation of distorted mixed crystals, as long as these are energetically feasible, with subsequent *phase transformation* to the product lattice, often followed by disintegration of the crystal. Different faces of the same crystal give different features and different reactivity. Molecular steps proved to be genuine crystal faces at the resolving power of the AFM. Thus, a completely new view of solid-state reactivity emerges and numerous new applications in waste-free quantitative syntheses without solvents or liquid phases were developed. Solid-state reactions are now close to prediction on the basis of sound experimental facts and improved theories, and will be the syntheses of the future, for the sake of economy, ecology, and environmental protection. We give here a review on recent developments and point to applications in various fields of chemistry and physics.

EXPERIMENTAL

All gas/solid-reactions were performed on a preparative scale by evacuating 2 - 5 mmole of ground crystals in round-bottomed flasks of the appropriate volume. The gas was sampled in a vacuum line at initially 1 bar (0.7 bar in the case of NO_2 and sampling by weight) to 1.1 - 2.0 times the stoichiometric quantity. After standing over night (most reactions were probably completed in shorter time periods) the excess gas was condensed under vacuum into a cooled flask (77 K) and the conversion, structure and purity of the product determined by the usual spectroscopic (IR, NMR, MS) and analytic techniques including DSC and TGA. In this paper

only uniform and quantitative reactions were chosen for mechanistic investigation with the AFM. AFM measurements with non-scraping tips and imaging techniques have been described elsewhere.[1] Nanophotolysis of 9-chloroanthracene 3 with an uncoated glass fiber SNOM-tip at a nominal aperture of 20 nm was performed at DME, Kopenhagen using 488 nm light in a Rasterscope 4000 SNOM. 10 μm topographies were scanned at a rate of 50 μm/s. The solid state UV/VIS-spectrum of 3 was recorded by diffuse reflection spectroscopy using an Ulbricht sphere attached to a Perkin Elmer Lambda 551S spectrometer. The long wavelength absorption onset was at about 550 nm. BET surfaces were measured with krypton, true densities with helium, both at a Denarmat of Stroehlein.

PHOTOREACTIONS

A review has appeared on the application of AFM and other SXM-techniques to the photochemistry of solids including polymers.[2] Both topochemically allowed and forbidden non-topotactic solid-state photolyses proceed with long range feature-forming molecular movements. The anisotropies of such movements are face-dependend. The new principle of phase rebuilding[2] and a more elaborate use of crystal packings than in common topochemistry[3] which did not foresee face-dependend movements over tens and hundreds of nm, is able to provide sound reasons for solid-state reactivity, both in topochemically "allowed" and "forbidden" reactions. The wealth of advancement made is particularly evident with *E/Z*-photoisomerizations in the crystal, which are summarized in Ref.2. A striking example is the photoisomerization of 1 to give 2.

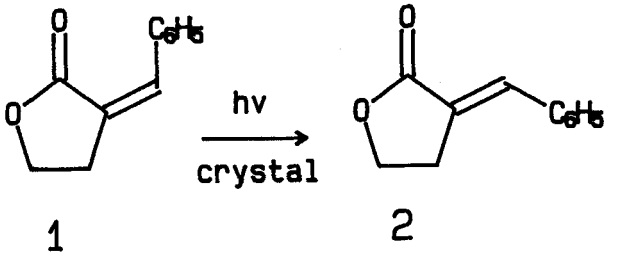

1 2

The crystal structure of 1[4] leaves enough space for cooperative bond rotation while avoiding severe van-der-Waals interactions. Phase rebuilding can start to produce craters on (010) and egg-box like features on (001)[2]. The reaction is very efficient on both faces and the phase transformation into the lattice of the product 2 leads to crystallites with heights in the μm-range which grow epitactically around the initial crystal, parallel to the c-axis on (010) and parallel to the b-axis on (001). Figure 1 shows the early and the later stages of the *E/Z*-photoisomerization on both faces.

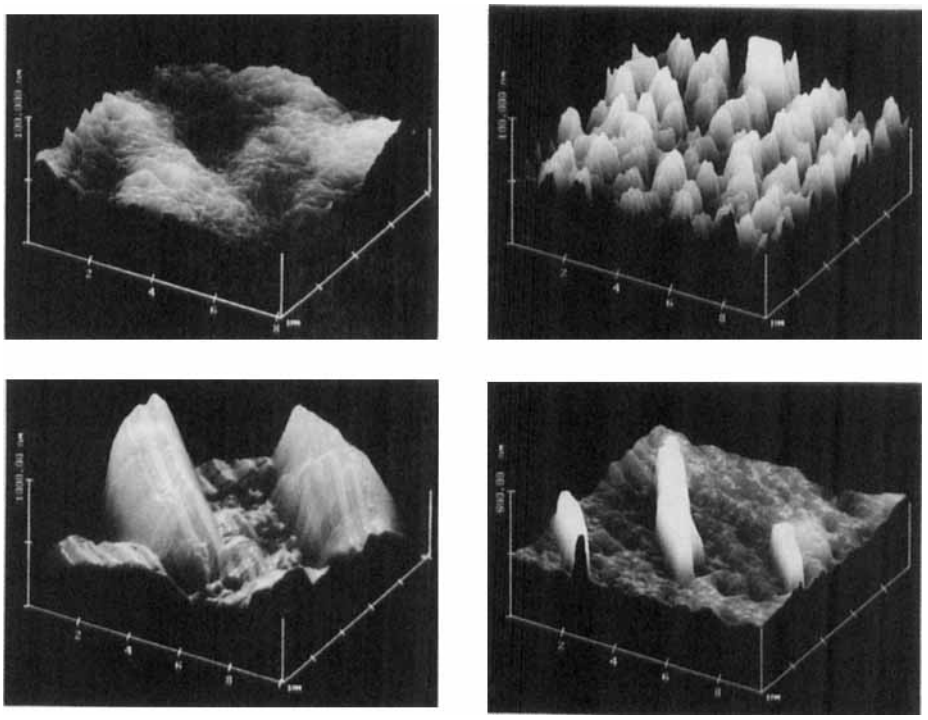

FIGURE 1 AFM-topography of the irradiation (>300 nm) of 1 ($P2_1/c$) to give 2; top left 30 s on (010); bottom left 100 s on (010), edges parallel to original c-axis; top right 15 s on (001); bottom right 45 s on (001), edges parallel to original b-axis.

Epitaxial growth in planes parallel to (100) after the preceding phase rebuilding apparently memorizes the original

crystal packing, the initial light penetration depth (90% at 365 nm) being about 480 nm. All oxygen atoms of the molecules 1 are located in planes parallel to (100) of its crystal according to its structure.[4] The molecules 2 use that site for concentrating their oxygens there, as well.

PHOTOREACTION USING SNOM TIPS

Scanning near field optical microscopy (SNOM) uses pipette tips as waveguides with very low apertures at their ends (e.g. 50 or 20 nm).[2,5] The local light intensities in working SNOM setups are in the order of several hundred quanta/sÅ^2.[6] Thus, some photochemistry will occur if the light is absorbed and the scanning is slow and even more so, if the pipette tip is not metal-coated and thus provides increased light emission over a larger spot by leakage through the side walls close to the aperture. Furthermore since metal-coated pipette tips become very hot at their ends they often experience erratic detachment of the coating upon use. Thus, it is important to use the feature-forming solid-state photochemistry for the investigation and control of the pipette tip performance. The photodimerization of 9-chloroanthracene 3 on its long side face to give dimer 4 was chosen for the first demonstration of such application in SNOM experiments, because the volcanoes formed upon ordinary irradiation (>300 nm) are uniformly spread over that surface (see Fig. 16 in Ref. 2). The 488 nm light of an argon-ion laser is absorbed by solid 3. An uncoated pipette tip of the Rasterscope 4000 SNOM in reflection-back-through-the-tip mode with a 20 nm aperture gave the up to 200 nm high features of Figure 2 when set in the near field at preselected sites and keeping it there for 20 min . It is seen that the features which have been generated by 3 different local near field irradiations are up to 2.5 μm wide and of irregular shape, although the influence of the initial roughness on 3 is of minor importance. Rather it is seen that the volcano-

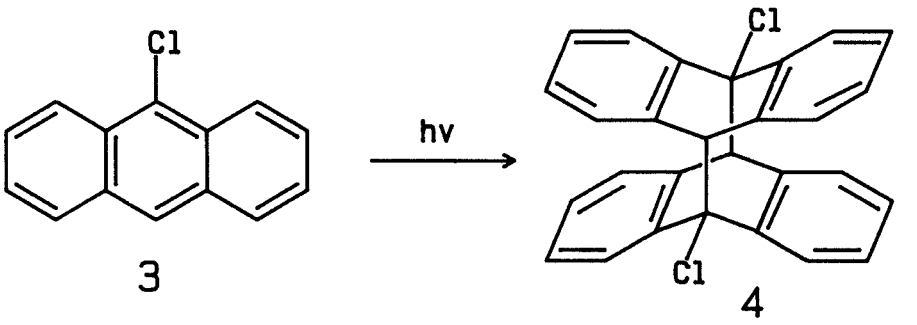

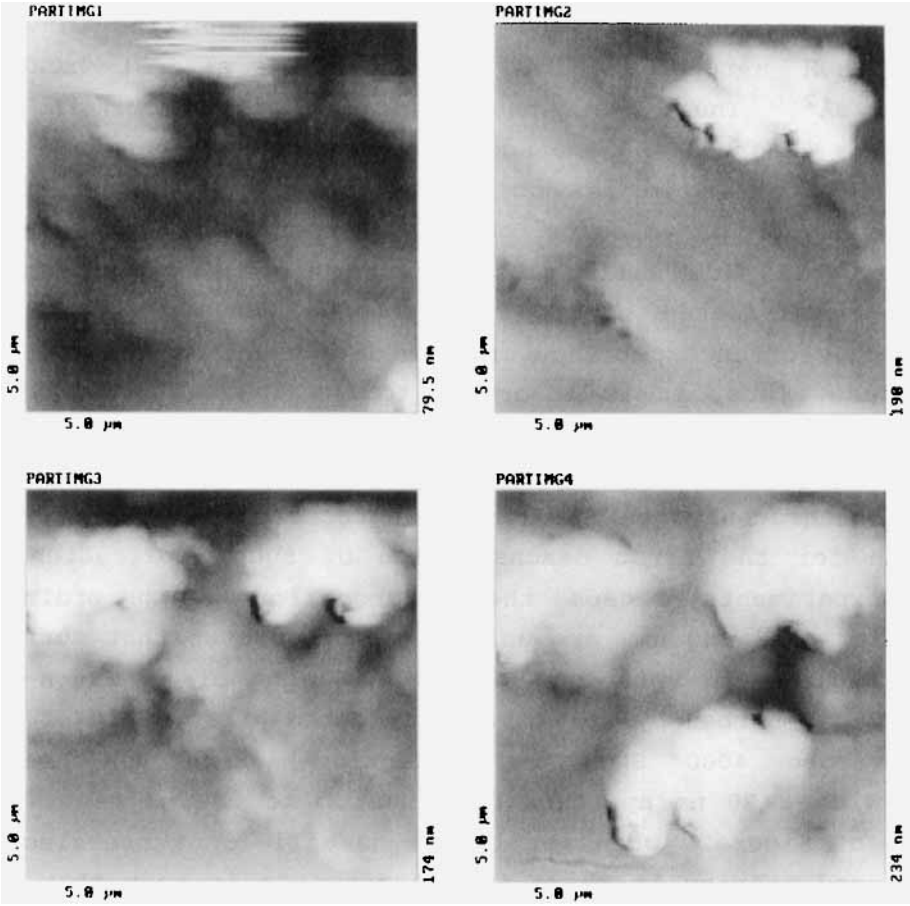

FIGURE 2 Non-contact AFM topography of the long side face of 3 without treatment and after placing the illuminated aperture for 20 min at 10 nm distance to the top right position, then to the left one, and finally midway to the bottom; all images are a quarter of 10 µm x 10 µm scans; the Z-scale has been set automatically.

type phase rebuilding mechanisms applies as in common irradiations, and that the leakage of light through the conical side walls of the pipette tip is rather wide with sharp limits (roughly 2.5 μm x 1.8 μm). The asymmetry of the steep (typically 40°) features proves that the luminosity around the cone was not circular, probably because the present tip had an oval cross-section and some defect on its front side. The application of this new technique to the control of uncoated and coated SNOM-tips as well as for local nano-photochemistry is promising and being studied further.

GAS/SOLID IMBIBITION

Clathrates are usually produced from solutions. Toda used the chiral host (*R*,*R*)-5 for liquid into crystal imbibition in the resolution of racemic compounds such as 6.[7]

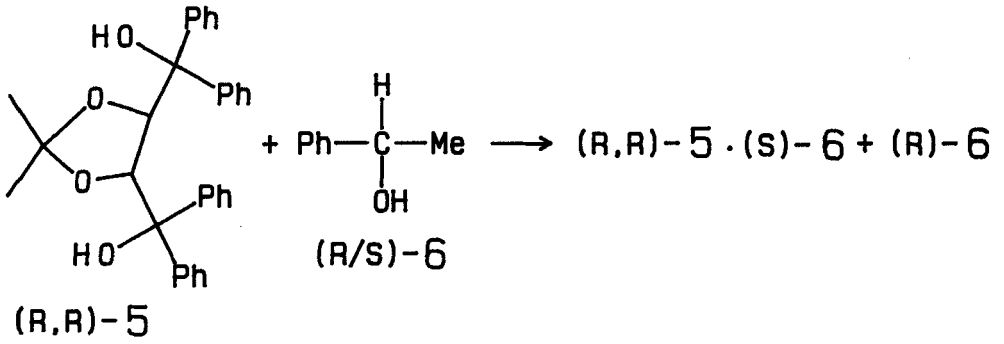

Such clathration usually alters the crystal lattice of the host and should therefore exhibit a phase rebuilding with long range movements of molecules and feature-formation.[8] Experimental proof by AFM measurements could be only achieved in gas/solid imbibition experiments because the problems of solubility/redeposition in saturated suspension media could not be settled for the molecular AFM sensitivity. The imbibition from the gas phase starting with a rather flat surface gives floes with some peaks on them orientated along the large crystal axis (Figure 3). Orientation along c is easily comprehended. Thus, the (010) plane cuts (100) ortho-

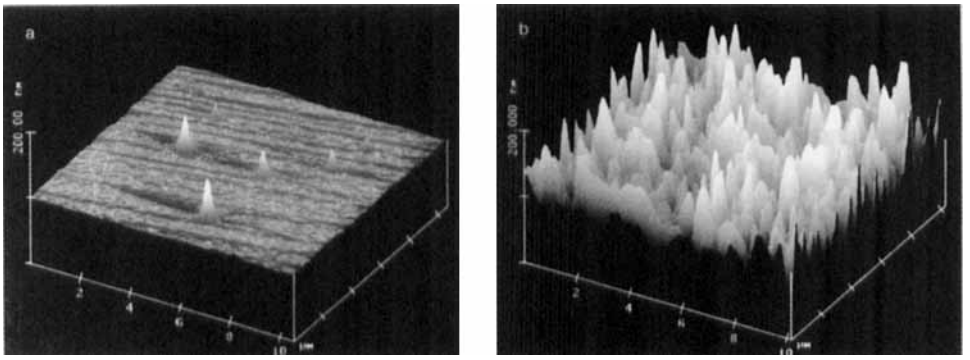

FIGURE 3 AFM topography of the main face of (*R*,*R*)-5 (P1, needles); (a) fresh; (b) after 2 h in a vacuum under saturation pressure of (*S*)-6 at 25°C.

gonally in c-direction and it is a cleavage plane due to the fact that double layers with the polar groups *in* and the phenyl groups *out* alternate under it.

The data show, that the mechanism of clathrate formation does not principally differ from those of solid-state chemical reactions. The gas/solid imbibition into (*R*,*R*)-5 may be used preparatively to remove traces of (*S*)-6 from the not imbibed (*R*)-6. Further examples of gas/solid imbibitions have been reported and summarized recently.[8]

SALT FORMATION

Acidic gases

The gas/solid technique is useful for the synthesis of salts if strong or weak solid N-bases (liquid ones might be solidified at low temperatures) are exposed to gaseous HCl, HBr, or HI.[8] Solid hydrohalides are formed most easily by this technique, dibases form dihydrohalides quantitatively and the products are more easily handled than the ones formed in low yield after laborious procedures from solutions. The basic amino acid (*L*)-histidine 7 forms a dihydrochloride with gaseous HCl. The AFM investigation on the (001) face of the orthorhombic modification of 7 shows the formation of huge heights and valleys (Figure 4). We see

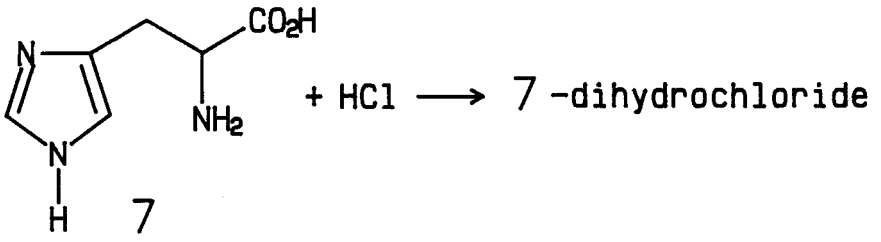

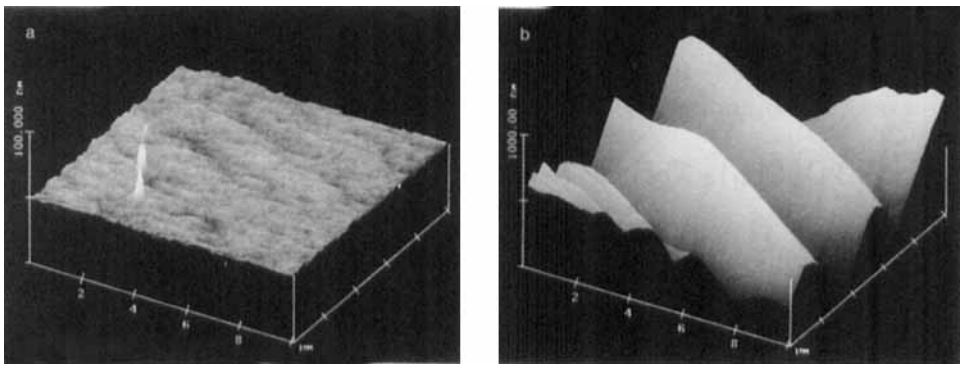

FIGURE 4 AFM topography of (*L*)-histidine 7 (from water, $P2_12_12_1$)[9] on (001); (a) prior to exposure; (b) after exposure to HCl gas, the rims being parallel to the a-axis of the crystal unit cell.

here, most likely, not the primary step (phase rebuilding) but the phase transformed stage already, due to very rapid reaction. (*L*)-Histidine has layers of infinite H-bonded strings which form less densely packed cleavage planes parallel to (010). Thus, the orientation of the features along the a-axis is comprehensible. The very large features explain themselves from an unusually large (42.5%) volume increase (increase in mass and density is 46% and 2.8%). In a preparative transformation, the specific surface increased from 0.083 to 0.67 m^2/g. The crystals disintegrate.

Basic gases

The reaction of carboxylic acids and phenols with ammonia and amines has been studied by Curtin, Paul, and Miller

using X-ray data, light microscopy, and solid-state NMR.[10] Anisotropic behavior has been observed under the light microscope. However frequently the anisotropies which had been predicted from X-ray structures could not be found experimentally by these techniques and discussion of that failure had to be postponed. Thus, it was not possible to explain the "extraordinary" behavior of adipic acid.[10] In all of these previous studies the concept of phase rebuilding was, of course, unknown. The submicroscopic probing of gas/solid reactions with the AFM is by far superior to the previous techniques, because it is able to view all events on the nm- up to the μm-scale.

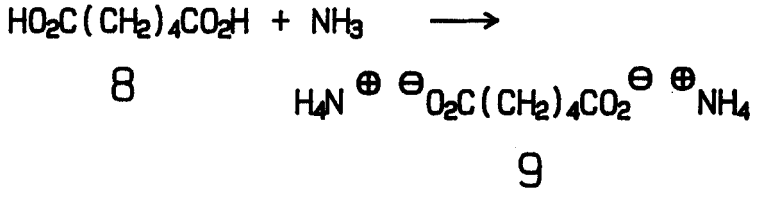

8 9

Solid adipic acid **8** and ammonia form the bisammonium salt **9** quantitatively. We see a very rapid reaction on (010) with egg-box like features at the phase rebuilding stage and phase transformation forming 1.6 μm high features (Figure 5a-c), whereas on (100) the rapidly formed volcano type features stay at a height of about 40 nm and do not increase any further even if 12 times as much of ammonia is applied (Figure 5d-f). Actually it is very hard to find some minor differences in the Figures 5e and 5f. Clearly, we have passivation on that face after formation of the nanofeatures which, of course, cannot be observed with a light microscope. The passivation on (100) points to an inability of phase transformation on that surface. The crystal packing (Figure 6) shows easily accessible carboxylic groups on both faces. However, penetration of the reaction into the crystal under (100) is difficult because of the infinite strings of hydrogen-bonded diacids. Thus, the reaction may come to a stop after reaction of a few molecular layers. On the other

hand under (010) the strings are broken up from their sides and the final phase transformation will not be hindered.

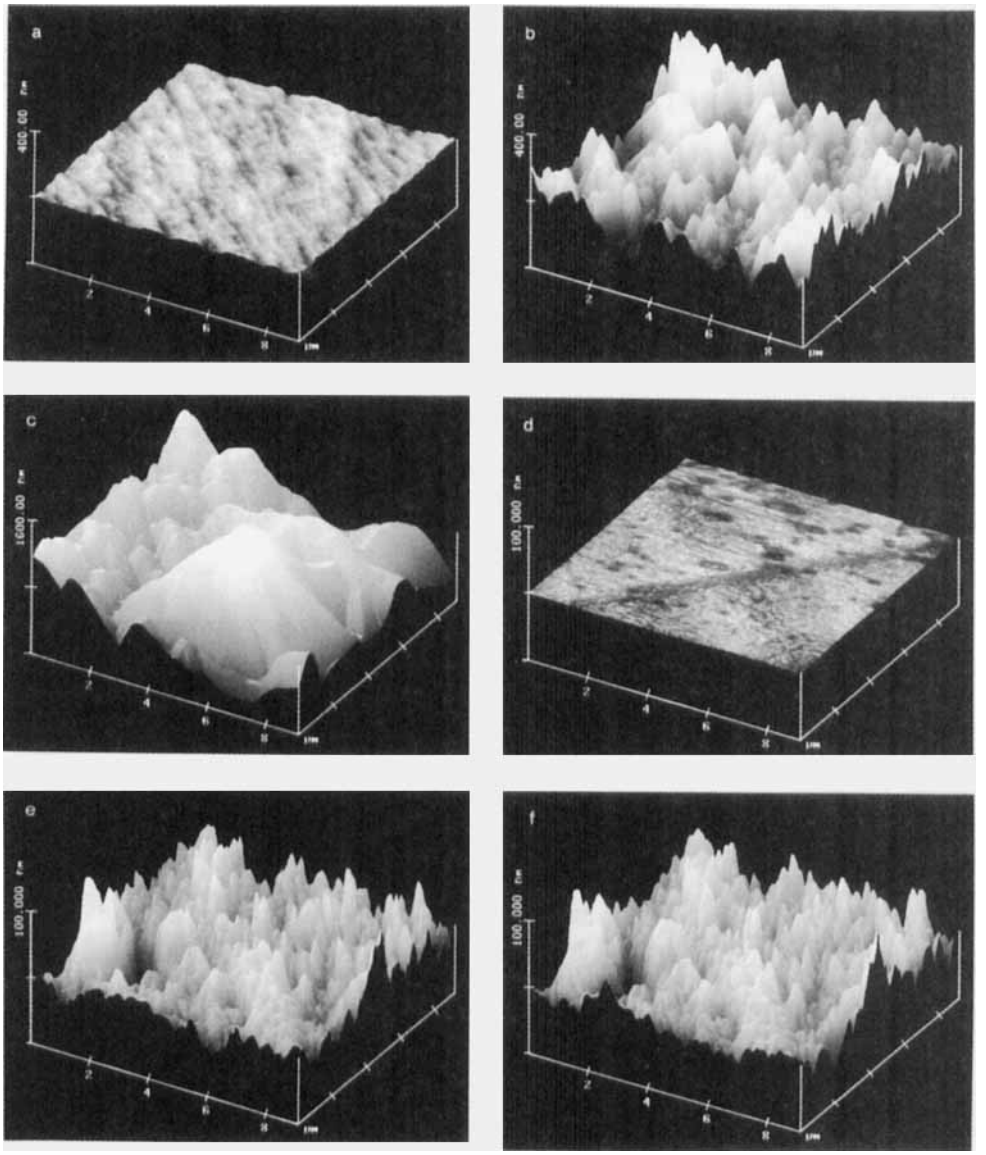

FIGURE 5 AFM topographies of adipic acid 8 from ethanol; (a) (010) surface, fresh; (b) (010) after application of 0.1 ml NH_3; (c) (010) + 0.2 ml NH_3; (d) (100) surface, fresh; (e) (100) + 0.05 ml NH_3; (f) (100) + 6 ml NH_3; the NH_3 was applied directly under the AFM head.

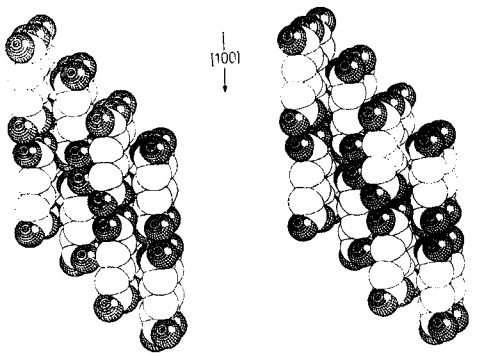

FIGURE 6 Stereoscopic view of the crystal packing of **8** ($P2_1/c$)[11] looking on (010) with (100) on the top slope, showing the strings of hydrogen-bonded molecules and the easy accessibility of the carboxylic acid groups; all O grid.

Also solid furane-2-carboxylic acid **10** reacts quantitatively with NH_3 gas to give its ammonium salt **11**. Again the sequence of phase rebuilding and phase transformation is easily seen in the AFM images on (100) of **10**. The volcanoes formed are several hundred nm high. Finally they reach the height of 1 μm while growing together. According to crystal structure[12] the dimer pairs of H-bonded molecules **10** stand

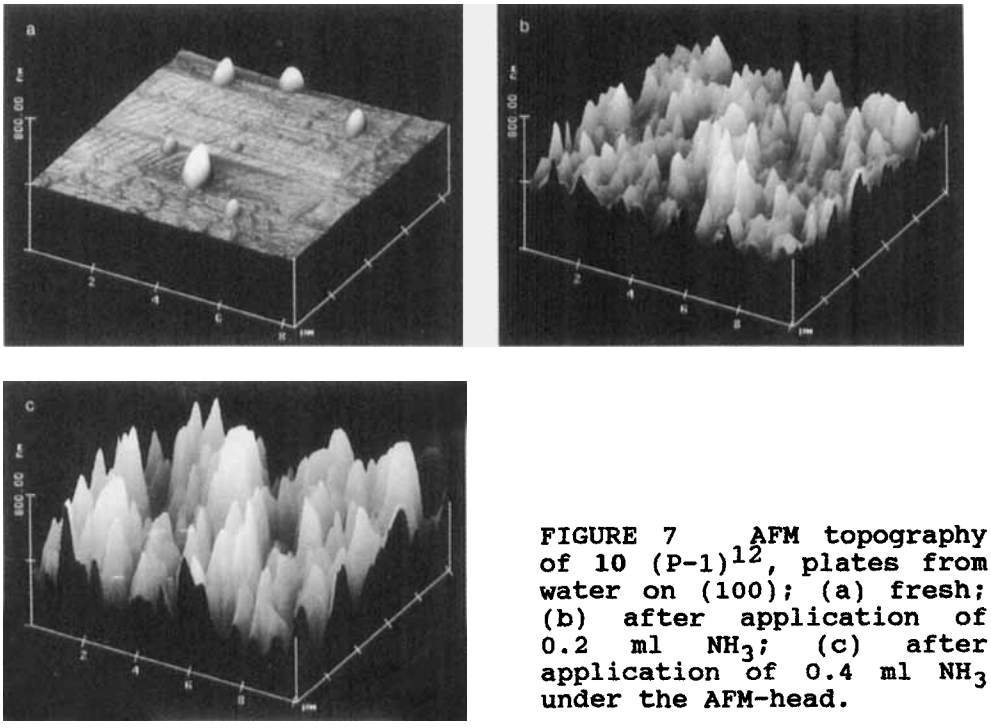

FIGURE 7 AFM topography of **10** (P-1)[12], plates from water on (100); (a) fresh; (b) after application of 0.2 ml NH_3; (c) after application of 0.4 ml NH_3 under the AFM-head.

steeply (86°) under (100) without interlocking. Therefore the formation of volcanoes by upward transport due to increase in density (2.7%), mass (15%) and volume (12%) is comprehensible and passivation does not occur. Upon prolonged reaction the crystals disintegrate, and after completion of the reaction an increase of the specific surface from 0.037 to 0.155 m^2/g has been measured.

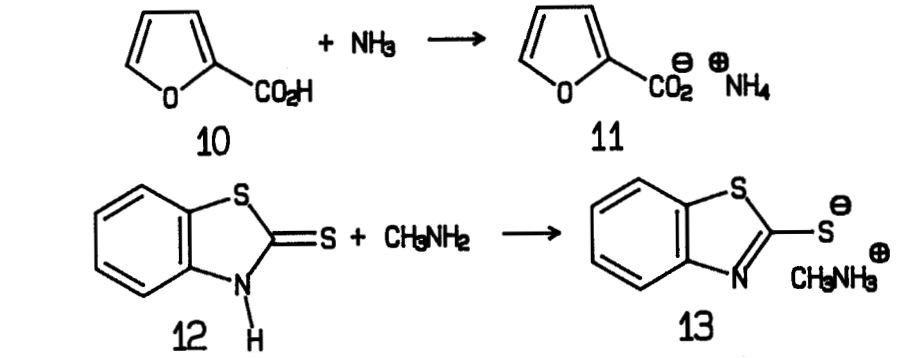

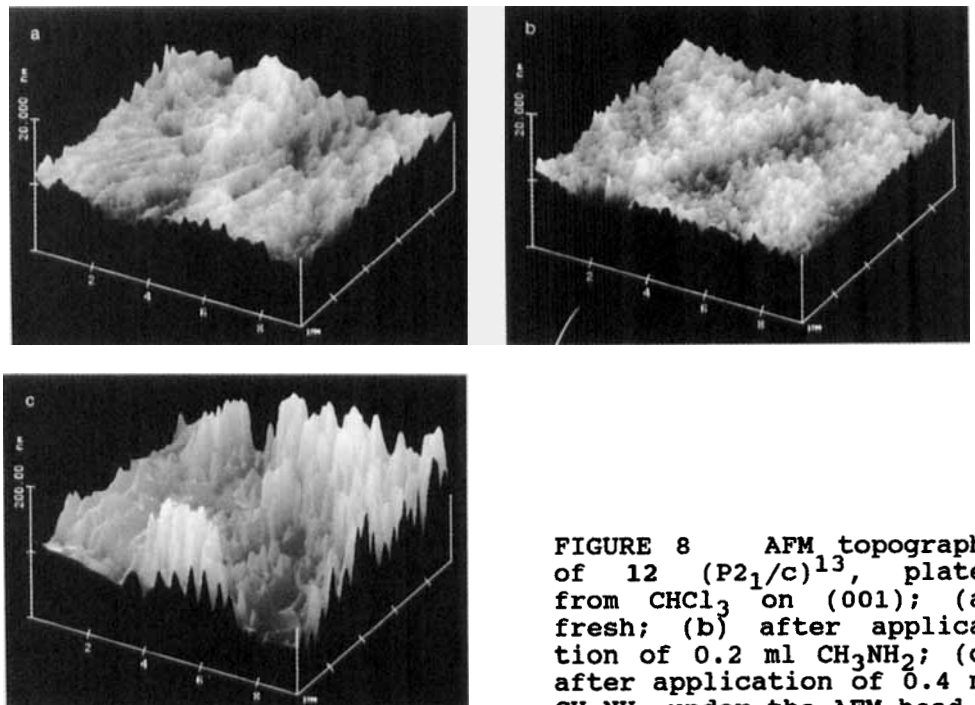

FIGURE 8 AFM topography of 12 $(P2_1/c)^{13}$, plates from $CHCl_3$ on (001); (a) fresh; (b) after application of 0.2 ml CH_3NH_2; (c) after application of 0.4 ml CH_3NH_2 under the AFM-head.

From a preparative point of view the formation of ammonium salts of very weak acids is even more important, because those are hardly available from solution. A striking example is 2-mercaptobenzothiazole which crystallizes in its thione form **12** and forms its methylammonium salt **13** quantitatively upon exposure of the crystals to gaseous methylamine at RT. In this salt formation the molecular steps on the surface disappear upon initial phase rebuilding (flattening in Figure 8 b), however, upon continuation of the reaction high clusters of pillars and floes form (Figure 8c). The molecules of **12** lie flatly (35°) in H-bonded double layers under (001) and these arrange in a zigzag. Therefore, the functional groups are shielded by the benzene rings and after reaction flat product covers out of **13** are accommodated. Only upon further reaction internal pressure, created by volume increase, is released by local rupture of the initial flat covers to form the diverse features of Figure 8c

HALOGENATION

The first reported gas/solid reaction was the addition of Br_2 to cinnamic acid.[14] Several reactions of that type followed only recently and some of them were studied in detail by AFM.[1] From a preparative point of view waste-free syntheses of labile products are rewarding. Gas/solid techniques are well suited and the highly functionalized dichloride **15** can be obtained quantitatively from the alkene **14** and gaseous Cl_2. **14** looses HCl in solution and Cl_2 upon heating to 230°C. Single crystals of **14** have been chlorinated.

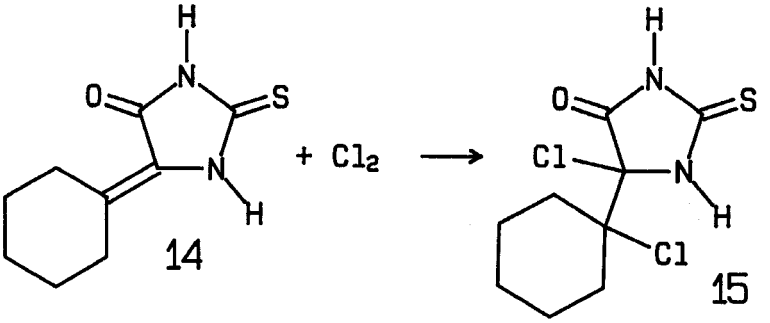

14 15

Figure 9 shows that no liquid is formed on the surface (stable images, see Refs. 1, 2, 8). Initially small craters (15 - 30 nm deep, 200 nm wide) form from a rather rough surface. 2 shots of 0.5 ml Cl_2 were applied with a syringe under a hood and immediately blown away, to give Figure 9b still in the range of phase rebuilding. However, an additional shot of 0.5 ml Cl_2 provoked the formation of very high

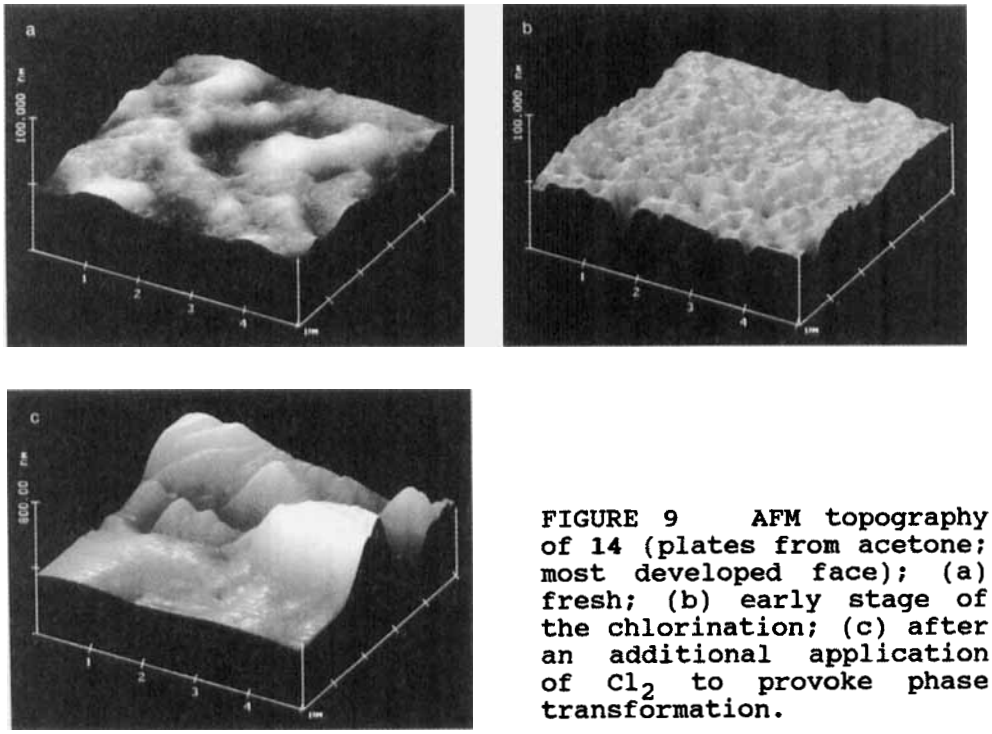

FIGURE 9 AFM topography of 14 (plates from acetone; most developed face); (a) fresh; (b) early stage of the chlorination; (c) after an additional application of Cl_2 to provoke phase transformation.

features obviously by phase transformation to the lattice of 15 (Figure 9c). After continuation of the reaction the crystal breaks into parts. The increases in mass, density, volume, and specific surface have been measured to be 36%, 15% 18% and 186%, respectively, of the starting values with 14.

GAS/SOLID-DIAZOTATION

Numerous types of gas/solid reactions of aromatic and heterocyclic compounds have been reported recently.[15] We now switched to primary aromatic amines.

While diazotations of aromatic amines in acid solutions have been the key step in azo-dye production and in the diverse applications of diazonium salts, the possibility for the synthesis of solid diazonium salts by gas/solid reaction has only recently been considered.[16] Thus, crystalline sulfanilic acid (monohydrate) **16c** and gaseous nitrogen dioxide formed the diazonium betaine (and HNO_3) quantitatively. AFM-studies on the (010) surface indicated phase rebuilding with formation of irregular flat islands which were related to the molecular packing. The water of reaction was not released from the reacting crystal.[16]

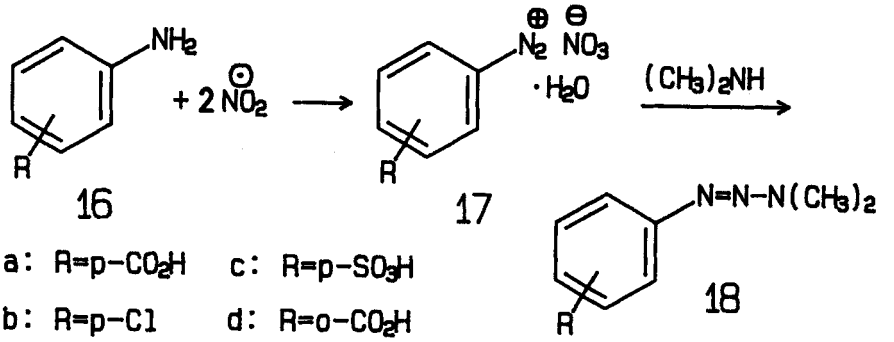

Similarly the crystals of *p*-aminobenzoic acid **16a**, *p*-chloroaniline **16b** and anthranilic acid **16d** react with NO_2 gas without melting to give the solid diazoniumnitrate hydrates **17** in quantitative yield. These solids may be used for further gas/solid reactions with aliphatic amines to give solid triazenes (e.g. **18**) or for reactions of **17** in non acidic or anhydrous (after drying) organic media. The diazotations require a complex series of reaction steps but proceed nevertheless quantitatively with the formation of crystalline nitrates which keep the water of reaction in their lattices. Furthermore, triazene formation by combination of **17** with residual **16** is reversible. The

reactions have been routinely performed on the gram scale but the details of thermal dehydration have not been studied by TGA because of the potential for explosions of such salts which can be easily demonstrated on an anvil when **2** is heavily hit with a hammer. However, grinding of **17a - d** for IR-measurements did not pose any problems. The triazenes **18**, which have also been obtained in solution,[17] are quantitatively formed if gaseous dimethylamine is applied to solid **17** after evaporation of excess NO_2. That reaction sequence underlines the synthetic potential: *wastes are avoided*.

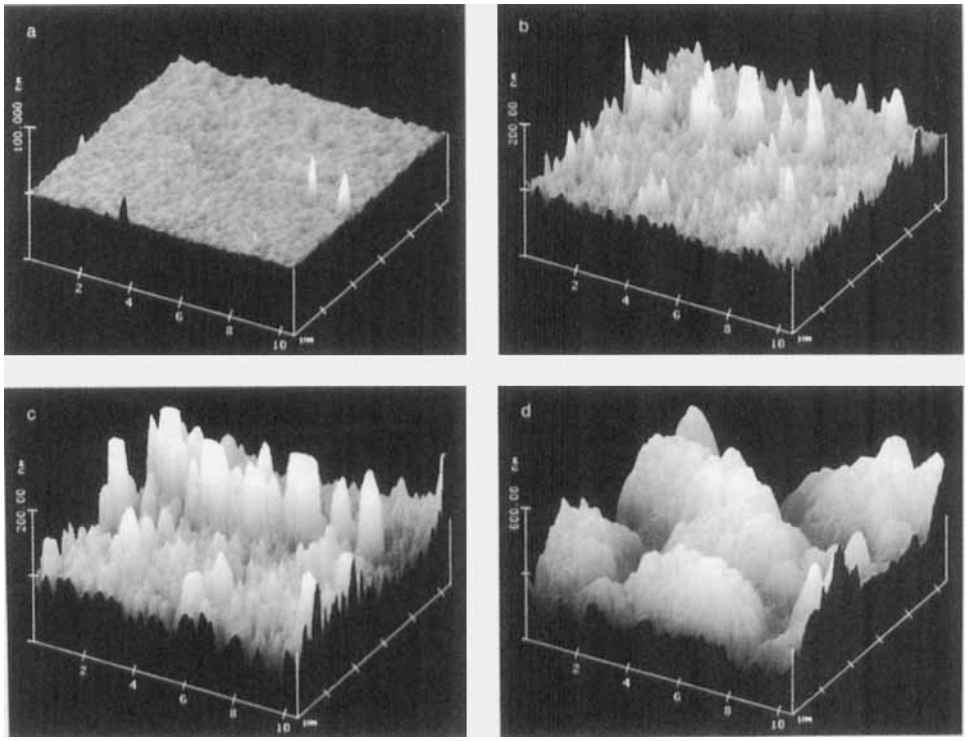

FIGURE 10 AFM images of the solid state diazotation of *p*-aminobenzoic acid **16a** ($P2_1/n$) on {101}[18] showing (a) a rather flat natural surface, (b) volcano formation all over the surface after short exposure to NO_2, (c) increase of the features upon doubled exposure, and (d) formation of very large compact features after tripled exposure.

The success of solid-state diazotations is the result of phase rebuilding with long range feature-forming molecular movements. Figure 10 shows the results of the AFM investigation of *p*-aminobenzoic acid on {101}. It is seen that the volcano-forming phase rebuilding starts quite uniformly over the whole previously flat surface, that the features increase, and that at a certain point the phase transformation forms the very large compact hills of Figure 10d. According to crystal structure the molecules **16a** stand steeply (72°) on their long side under (101), taking various skew positions (Figure 11). Therefore, the common volcano mechanism with upward transport upon chemical reaction is not surprising. Interlocking is the reason for the lack of lateral orientation (one row obviously by chance in Figure 10) during phase rebuilding and phase transformation. At the stage of Figure 10d the crystal starts to disintegrate.

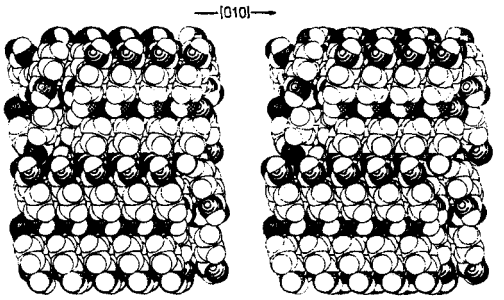

FIGURE 11 Stereoscopic space filling representation of the molecular packing of **16a** ($P2_1/n$, from ethanol) on its pinacoid {101}; N grids; O circles.

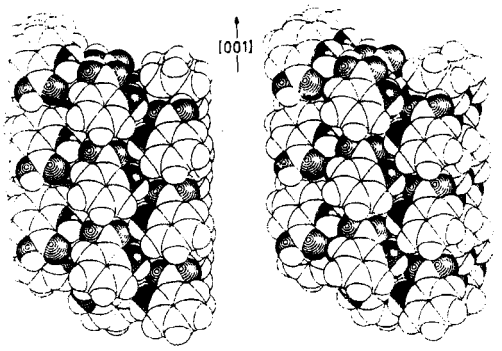

FIGURE 12 Stereoscopic space filling representation of the molecular packing of **16d** (Pbca)[19] on (100) showing flat lying molecules (32°) forming H-bonded layers with shielding of the NH_2 groups.

The crystal lattice of anthranilic acid **16d**[19] is different to the one of **16a**. Molecular layers form with a maximum of

hydrogen bonds (Figure 12) and the amino groups, subject to diazotation, are not readily available at the dominant (100) surface. Therefore it is easier to approach the NO_2 molecules from faces which are vertical or steep to (100) (see e.g. the {001}-forms of Figure 12). That expectation is clearly met in the AFM-images of Figure 13. The initial crystals which had been grown from ethanol exhibit several submicroscopic craters, the slopes of which being faces which are vertical or steep with respect to (100). It is seen, that diazotation starts in those submicroscopic craters (diameters up to 500 nm, depths down to 140 nm). They become larger in (b) (typically 1.5 μm diameters, depths down to 140 nm) and very large in (c) (diamters up to 3 μm, depths down to 90 nm) with flat bottoms. Also vertical transport of material due to mass increase is discernible at the walls with "swallowing" of smaller features. In (c) are seen indications of flattening due to phase transformation. Clearly the craters derive from the crystal structure.

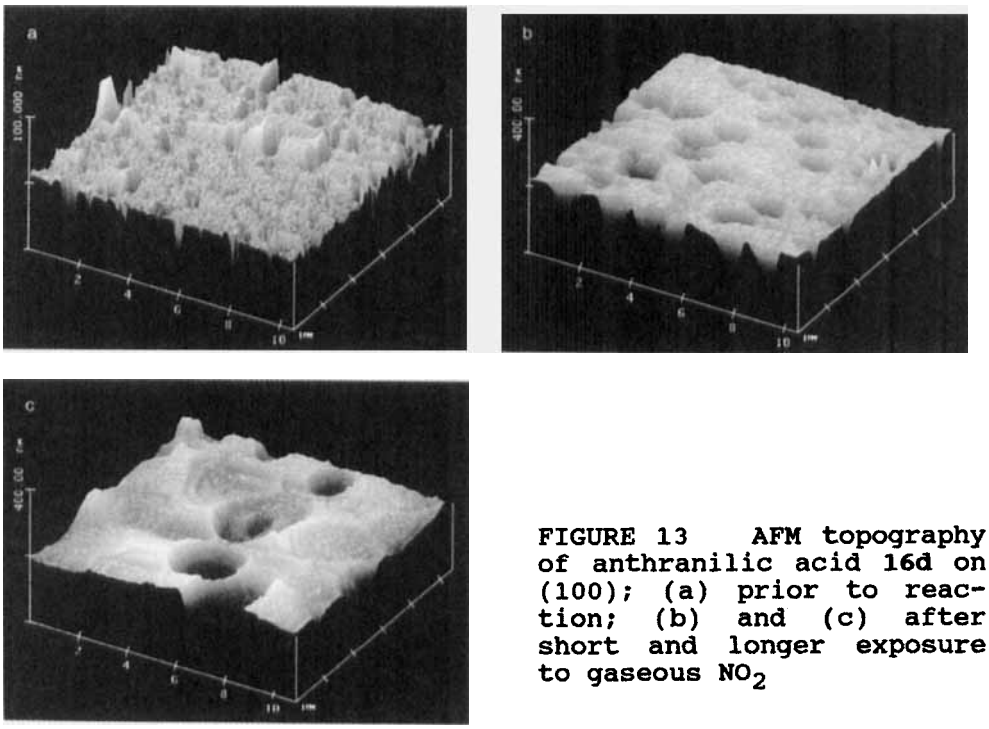

FIGURE 13 AFM topography of anthranilic acid 16d on (100); (a) prior to reaction; (b) and (c) after short and longer exposure to gaseous NO_2

SOLID/SOLID REACTIONS

Solid/solid reactions have been developed and summarized by Toda and coworkers.[20] Their potential for waste-free syntheses makes them interesting in particular if they stay solid during reaction. The first mechanistic study with the AFM has been performed with benzopinacol **19** and *p*-toluenesulfonic acid monohydrate **20** to give **21** and H_2O.[21] It turned out, that the water of reaction which is released in that pinacol rearrangement has to be continuously evaporated to increase the rate and obtain 100% yield. Thus the water is impeding, not facilitating. The AFM study revealed no reaction on (001) of benzopinacol **19** but distance dependend crater formation on the (100) face with charge separations over 2 mm, because the catalytic protons which enter via (100) by protonation of suitably orientated hydroxyl groups form water at one side of a crystal compartment with the consequence of liberation of a new proton on the other side in the next compartment etc. The nonreactivity of **19** on (001) derives from unfavorable orientation of the hydroxyl groups with their hydrogens (rather than electron pairs) pointing outward and thus impeding protonation.

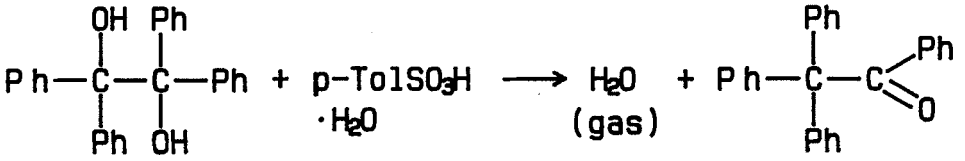

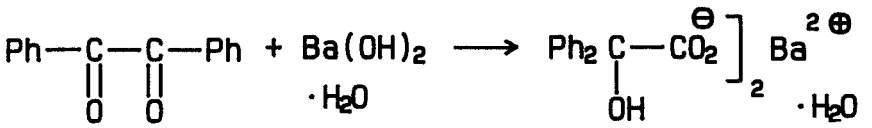

Of similar interest is the solid/solid benzilic acid rearrangement of benzil **22** with (non hygroscopic)

$Ba(OH)_2 \cdot H_2O$.[20] to give 23. The reaction runs at 80°C which is close to the melting point of sublimed 22 (95 - 97°C). However, AFM may recognize intermediate submicromelting if it occurs. The (001)-face of trigonal 22 is unchanged under the AFM if it is heated to 90°C for 3 h. However, if a tiny crystal of $Ba(OH)_2 \cdot H_2O$ is laid down on that face and the AFM image scanned after 3 h of previous heating to 80°C, the valleys and composite heights of Figure 14b ensue and align themselves parallel. These features occur at the minimal working distance of about 3 μm from the tiny crystal (standard tip) up to the edges of 0.8 mm wide crystals 22. The orientation of the ridges and valleys stays undetermined on a triangular (001)-plane with alternating layers related by rotations of 0°, 120°, and 240°. It may happen that the orientation of the steep halves (71°) of the bent molecules (109°) in the upmost layer determines the direction and that

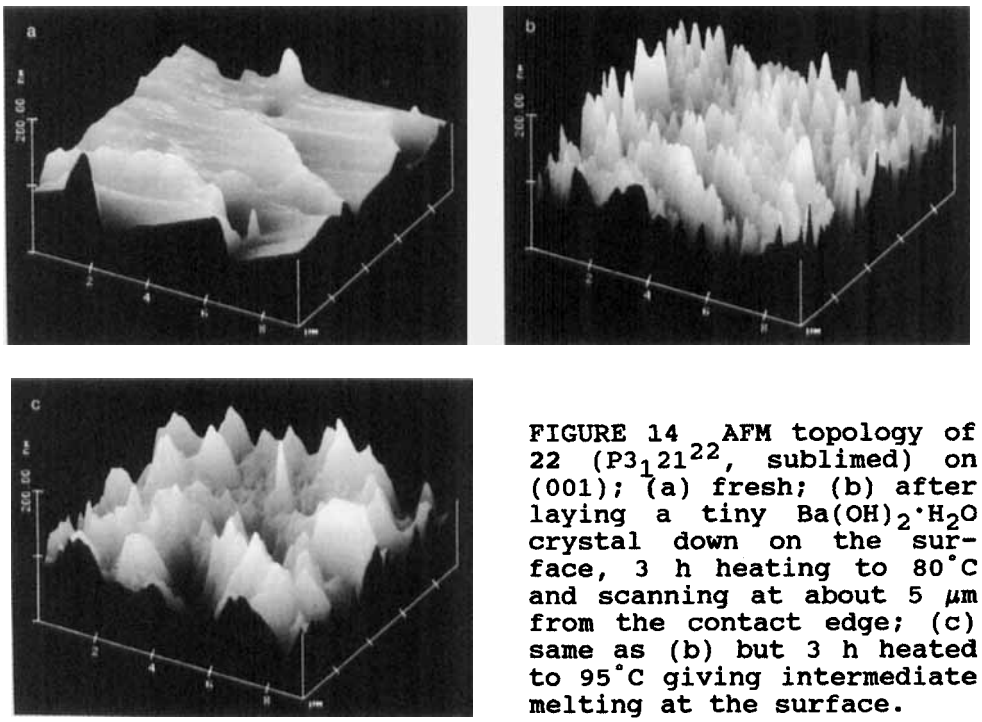

FIGURE 14 AFM topology of 22 ($P3_121$[22], sublimed) on (001); (a) fresh; (b) after laying a tiny $Ba(OH)_2 \cdot H_2O$ crystal down on the surface, 3 h heating to 80°C and scanning at about 5 μm from the contact edge; (c) same as (b) but 3 h heated to 95°C giving intermediate melting at the surface.

this one is then followed by the deeper molecules when they react. However, further studies will have to evaluate more details, in particular concerning the migrations of the OH^- and Ba^{2+} ions. The ridge to valley height is up to 200 nm; submicromelting did not occur at the surface of Figure 14b. An additional experiment was undertaken to show the influence of partial melting upon reaction with solid $Ba(OH)_2$. Thus, in Figure 14c are seen resolidified hills. The sample was here 3 h at 95°C, just at the melting point of 21. The features do not exhibit lateral orientation as in Figure 14b. Clearly, the influence of the crystal lattice has been lost by submicromelting in this experiment.

CONCLUSIONS

The AFM data reveal again[1,2] face-selective feature-forming long-range movements of molecules in (non-topotactic) solid-state reactions of all types. Phase rebuilding is clearly correlated with the molecular packing. Many new examples for different types of reactions have been developed. The possibilities for applications are manifold, predictability of further examples almost achieved. The mechanistic elucidations should now help with the acceptance and widespread application of waste-free new reaction techniques without solvents and without liquid phases. These techniques are badly needed for environmental protection.

ACKNOWLEDGEMENTS

This work has been supported in part by the Deutsche Forschungsgemeinschaft and the Fonds der Chemischen Industrie. We thank Steen Madsen for running the Rasterscope 4000 SNOM prototype of DME at The Technical University of Denmark in Kopenhagen, W. Saak is thanked for the determination of the Miller indices of the crystals of 22 and Prof. F. Toda for the crystals of (*R*,*R*)-5.

REFERENCES

1. G. Kaupp, Mol. Cryst. Liq. Cryst., 252, 259 (1994); 242, 153 (1994).
2. G. Kaupp, Adv. Photochem., 19, 119 (1995).
3. G. M. J. Schmidt, Pure Appl. Chem., 27, 647 (1971).
4. R. Boese, University of Essen, to be published.
5. D. W. Pohl in Advances in Optical and Electron Microscopy, C. J. R. Sheppard and T. Mulvey, Eds., Academic Press, London, 1990, p. 243.
6. D. A. McL. Smith, S. A. Williams, R. D. Miller, and R. M. Hochstrasser, J. Fluor., 4, 137 (1994).
7. F. Toda and Y. Tohi, J. Chem. Soc. Chem. Commun., 1993, 1238.
8. G. Kaupp, U. Pogodda, and J. Schmeyers, Chem. Ber., 127, 2249 (1994).
9. J. J. Madden, E. L. McGandy, and N.C. Seeman, Acta Cryst., B28, 2377 (1972).
10. R. S. Miller, D. Y. Curtin, and I. C. Paul, J. Am. Chem. Soc., 96, 6334 and 6340 (1974); I. C. Paul and D. Y. Curtin, Science, 187, 19 (1975); C. C. Chiang, C.-T. Lin, A. H.-J. Wang, D. Y. Curtin, and I. C. Paul, J. Am. Chem. Soc. 99, 6303 (1977); L. G. Butler, D. G. Cory, K. M. Dodey, J. B. Miller, and A. N. Gerroway, J. Am. Chem. Soc., 114, 125 (1992).
11. J. Housty and M. Hospital, Acta Cryst., 18, 693 (1965).
12. C. J. Gilmore, P. R. Mallinson, and J. C. Speakman, Acta Cryst., C39, 1111 (1983).
13. J. P. Chesick and J. Donohue, Acta Cryst., B27, 1441 (1971).
14. A. Schmitt, Liebigs Ann. Chem., 127, 319 (1863).
15. G. Kaupp and J. Schmeyers, J. Org. Chem., 60, issue 16 (1995).
16. G. Kaupp, J. Schmeyers, M. Haak, and A. Herrmann, Labo-Trend 95, Kennziffer-Fachzeitschrift für Labortechnik, 26, 57 (1995); for an English version including original color images and further reviews see WWW-publications, at http://kaupp.chemie.uni-oldenburg.de/~haak/ocI.html or via homepage of University of Oldenburg, there org. chemistry Kaupp, there electronic publishing.
17. Th. Axenrod, P. Mangiaracina, and P. S. Pregosin, Helv. Chim. Acta, 1976, 59.
18. T. F. Lai and R. E. Marsh, Acta Cryst., 22, 885 (1967).
19. C. J. Brown, Proc. Roy. Soc., A302, 185 (1986).
20. F. Toda in Reactivity in Molecular Crystals, Y Ohashi, Ed., Kodansha, Tokyo, 1993, p. 177.
21. G. Kaupp, M. Haak, and F. Toda, J. Phys. Org. Chem., 1995, in press.
22. E. S. Grabe, Y. LePage, F. L. Lee, and L. R. C. Barclay, Acta Cryst., B37, 197 (1981).